

International Journal of Modern Physics D
 © World Scientific Publishing Company

Radial Oscillations and Dynamical Instability Analysis for Linear GUP-modified White Dwarfs

JOHN PAUL R. BERNALDEZ

*Department of Physics, University of San Carlos, Nasipit, Talamban
 Cebu City, Cebu 6000, Philippines
 bernaldezjp@gmail.com*

ADRIAN G. ABAC

*Max Planck Institute for Gravitational Physics (Albert Einstein Institute), Am Mühlenberg 1,
 D-14476 Potsdam, Germany
 adrian.abac@aei.mpg.de*

*Department of Physics, University of San Carlos, Nasipit, Talamban
 Cebu City, Cebu 6000, Philippines*

ROLAND EMERITO S. OTADOY

*Department of Physics, University of San Carlos, Nasipit, Talamban
 Cebu City, Cebu 6000, Philippines
 rsotadoy@usc.edu.ph*

Received Day Month Year

Revised Day Month Year

A modification to the Heisenberg uncertainty principle is called the generalized uncertainty principle (GUP), which emerged due to the introduction of a minimum measurable length, common among phenomenological approaches to quantum gravity. An approach to GUP called linear GUP (LGUP) has recently been developed that satisfies both the minimum measurable length and the maximum measurable momentum, resulting to a phase space volume proportional to the first-order momentum $(1 - \alpha p)^{-4} d^3x d^3p$, where α is the still-unestablished GUP parameter. In this study, we explore the mass-radius relations of LGUP-modified white dwarfs, and provide them with radial perturbations to investigate the dynamical instability arising from the oscillations. We find from the mass-radius relations that LGUP results to a white dwarf with a lower maximum mass, and this effect gets more apparent with larger the values of α . We also observe that the mass of the white dwarf corresponding to the vanishing of the square of the fundamental frequency ω_0 is the maximum mass the white dwarf can have in the mass-radius relations. The dynamical instability analysis also shows that instability sets in for all values of the GUP parameters α , and at lower central densities ρ_c (corresponding to lower maximum masses) for increasing α , which verifies the results obtained from the mass-radius relations plots. Finally, we note that the mass limit is preserved for LGUP-modified white dwarfs, indicating that LGUP supports gravitational collapse of the compact object.

Keywords: neutron stars; GUP; mass-radius relation; equation of state.

PACS numbers:

1. Introduction

A modification to the fundamental commutation relation, which is predicted by several quantum gravity phenomenology approaches leads to the generalization of the Heisenberg's uncertainty principle (HUP). This modification to the HUP is called the generalized uncertainty principle (GUP), which emerged due to the introduction of a minimum measurable length.^{1,2} A specific approach to the generalized uncertainty principle, which satisfies not only black hole physics but also string theory and doubly special relativity (DSR), was developed and is called the "linear" GUP (LGUP) approach.¹⁻⁷ The LGUP approach satisfies both the minimum measurable length and the maximum measurable momentum conditions and is when the phase space volume is proportional to first-order momentum p , i.e. $(1 - \alpha p)^{-4} d^3x d^3p$, where α is the quantum gravity parameter, which has no established values and ranges from $10^{12} < \alpha_0 < 10^{24}$. LGUP has been studied and applied to numerous systems, such as the structure of compact objects like white dwarfs and neutron stars. Several studies which involve investigating the effects of LGUP on white dwarfs show that LGUP resists collapse, by increasing or completely removing their mass limit (Chandrasekhar mass), while other studies show LGUP supports collapse by reducing the maximum mass limit and increasing the minimum radius limit.¹⁻¹⁰

In the context of general relativity, which matters for the most massive white dwarfs, and where GUP effects are known to be most prominent, the dynamical instability of a white dwarf or a compact object can be investigated by studying its behavior under radial oscillations. This was done before in the context of the quadratic generalized uncertainty principle (QGUP) done by Ref. 11, where for the most part, QGUP resists gravitational collapse by increasing the Chandrasekhar mass limit. The GUP-modified equation of states prevents further gravitational collapse and limits the formation of compact astrophysical objects to that of the white dwarfs, which is in contrast with astrophysical observations, since heavier compact objects such as neutron stars exist. However, they find that dynamical instability can still set in on values of the $\beta_0 \leq 5.38 \times 10^{39}$,¹¹⁻¹⁵ where β_0 is the dimensionless QGUP parameter. Since it was shown by Ref. 1, 9, 10, that LGUP seems to supports to gravitational collapse, it is reasonable to explore dynamical instability on linear-GUP-modified white dwarf stars,^{1, 11-13} and to see whether this effect is present for a large range of values of the LGUP parameter.

We then present the main problem and objectives of this work - investigating dynamical instability for LGUP-modified white dwarfs. We take the framework of general relativity (GR) and calculate the stellar structure of the LGUP-modified white dwarfs, where we will obtain the exact forms of the linear GUP modified number density, energy density, and pressure of ideal Fermi gases at zero-temperature, and from there, a modified Chandrasekhar equation of state (EoS) will be formulated. This will then be used to obtain the analytical form of the LGUP-modified structure equations for zero-temperature white dwarfs, and their solutions will be analyzed along with those of the modified Tolman-Oppenheimer-Volkoff (TOV) structure

equations in general relativity (GR). From the structure equations, we obtain the modified mass-radius relation of the white dwarfs. We then carry out dynamical instability analysis on the LGUP-modified white dwarfs so that the maximal stable configuration of the system is identified. Finally, we present the conclusions and recommendations for future work.

2. Linear GUP-modified White Dwarfs

In this section, we review the Linear Generalized Uncertainty Principle (LGUP), as well as the statistical mechanics of Fermi gases modified by LGUP.

2.1. Generalized Uncertainty Principle

The generalized uncertainty principle (GUP) is a modification to the Heisenberg's uncertainty principle, which emerged due to the existence of a minimum measurable length. The fundamental commutation relation that satisfies both black hole physics and string theory is:^{1,18}

$$[x, p] = i\hbar(1 + \beta p^2), \quad (1)$$

which then results to the quadratic GUP given by:

$$\Delta x \Delta p \geq \frac{\hbar}{2} [1 + \beta(\Delta p)^2 + \langle p \rangle^2]. \quad (2)$$

Another approach to the general uncertainty principle, which not only satisfies black hole physics but also fits well with string theory, and doubly special relativity (DSR), was developed and is called the “linear” GUP (LGUP) approach, where the commutation relation is given by:

$$\begin{aligned} [x_i, p_j] &= i \left[\delta_{ij} - \alpha \left(p \delta_{ij} + \frac{p_i p_j}{p} \right) + \alpha^2 (p^2 \delta_{ij} + 3 p_i p_j) \right] \\ [x_i, x_j] &= [p_i, p_j] = 0 \end{aligned} \quad (3)$$

and the generalized uncertainty principle in one dimension is given by:

$$\Delta x \Delta p \geq \frac{\hbar}{2} [1 - 2\alpha \langle p \rangle + 4\alpha^2 \langle p \rangle^2], \quad (4)$$

where $\alpha = \frac{\alpha_0}{(M_p c)} = \alpha_0 \left(\frac{l_p}{\hbar} \right)$ is the GUP parameter.^{1,8–10} It should be noted that there are currently no established values for the GUP parameter α_0 . From Ref. 19, the upper bound of α_0 is suggested to be less than 10^{17} in order to be compatible with the electroweak theory. On the other hand, Ref. 20 suggests an upper bound for the GUP parameter of $\alpha_0 < 10^{24}$, in order to address the concerns with regards Landau energy shifts for particles that have a mass m and a charge e within a constant magnetic field and cyclotron frequency. The effects of linear GUP on the Lamb shift also suggest for a GUP parameter upper bound of $\alpha_0 < 10^{12}$. From Ref. 21, the gravitational wave event GW150914 suggests an upper bound of $\alpha_0 <$

4 Bernaldez, Abac, Otadoy

1.8×10^{20} . Thus, in order to maximize the effects of linear GUP as used similarly with Ref. 22, the GUP parameter values of 10^{17} , 10^{19} , 10^{20} , and 7×10^{20} will be used.

2.2. Statistical Mechanics of Fermionic Gases with LGUP Modification

Statistical mechanics plays an important role to understanding the structure of stars and compact objects since white dwarfs are generally composed of degenerate electron gases. With this, there is a need to derive the thermodynamic properties of the degenerate Fermi gas at zero temperature obeying Pauli's exclusion principle. We start with the grand canonical ensemble formalism in statistical mechanics in order to derive the relevant thermodynamic quantities, which are the number density n , energy density e , and pressure P .^{1, 9, 12, 23, 24} The partition function can be written as:^{1, 12, 23, 25}

$$\ln Z = \sum_j \ln[1 + e^{\frac{(\mu - E_j)}{k_B T}}]. \quad (5)$$

For large volumes, as modified by linear GUP, we then have:

$$\int \frac{d^3x d^3p}{(2\pi\hbar)^3} \rightarrow \int \frac{d^3x d^3p}{(2\pi\hbar)^3(1 - \alpha p)^4}. \quad (6)$$

Thus, the grand canonical potential can then be rewritten as:

$$\Phi = -gk_B T \int \frac{d^3x d^3p}{(2\pi\hbar)^3(1 - \alpha p)^4} \ln[1 + e^{\frac{(\mu - E)}{(k_B T)}}], \quad (7)$$

where g refers to the multiplicity of states due to the spin of the particle, and $(2\pi\hbar)^3$ refers to the volume occupied by and energy state in phase-space. From this, we then derive the expressions for the number density n , pressure P , electron energy density ϵ_e , and total energy density ϵ . The expression for number density, pressure, and electron energy density for degenerate ideal Fermi gases are given by:¹

$$n = \frac{8\pi}{(2\pi\hbar)^3} \int_0^{p_F} \frac{p^2 dp}{(1 - \alpha p)^4} \quad (8)$$

$$\epsilon_e = \frac{8\pi}{(2\pi\hbar)^3} \int_0^{p_F} E \frac{p^2 dp}{(1 - \alpha p)^4} \quad (9)$$

$$P = \frac{8\pi}{(2\pi\hbar)^3} \int_0^{p_F} (E_F - E) \frac{p^2 dp}{(1 - \alpha p)^4} = E_F n - \epsilon_e, \quad (10)$$

where p_F is the Fermi momentum, which corresponds to the maximum possible momentum, corresponding to the Fermi energy E_F in the zero-temperature case.

To optimize the numerical computation, we define a set of dimensionless quantities:

$$\begin{aligned}\xi &\equiv \frac{p_F}{m_e c} \\ \tilde{p} &\equiv \frac{p}{m_e c} \\ \sigma &\equiv m_e c \alpha\end{aligned}\tag{11}$$

Thus, equations (8)-(10) can be rewritten as:

$$n = \frac{\pi m_e^3 c^3}{(2\pi\hbar)^3} \int_0^\xi 8 \frac{\tilde{p}^2 d\tilde{p}}{(1 - \sigma\tilde{p})^4} = K\tilde{N}\tag{12}$$

$$\epsilon_e = \frac{\pi m_e^3 c^3}{(2\pi\hbar)^3} \int_0^\xi 8\tilde{E}_F \frac{\tilde{p}^2 d\tilde{p}}{(1 - \sigma\tilde{p})^4} = K\tilde{\epsilon}_e\tag{13}$$

$$P = \frac{\pi m_e^3 c^3}{(2\pi\hbar)^3} \int_0^\xi 8(\tilde{E}_F - \tilde{E}) \frac{\tilde{p}^2 d\tilde{p}}{(1 - \sigma\tilde{p})^4} = K\tilde{P},\tag{14}$$

where $\tilde{E} = \sqrt{1 + \tilde{p}^2}$, $\tilde{E}_F = \sqrt{1 + \xi^2}$, and $K = \frac{\pi m_e^3 c^3}{(2\pi\hbar)^3}$. \tilde{N} , $\tilde{\epsilon}_e$, and \tilde{P} refers to the dimensionless number density, dimensionless electron energy density, and dimensionless pressure respectively. Evaluating equations (12) and (14) yields the dimensionless equations:

$$\tilde{N}(\xi) = \frac{8\xi^3}{3(1 - \xi\sigma)^3}\tag{15}$$

$$\begin{aligned}\tilde{P}(\xi) = & \frac{1}{3\sigma^4} 4 \left\{ -2\sqrt{1 + \xi^2}\sigma - \frac{2\sqrt{1 + \xi^2}\sigma}{(-1 + \xi\sigma)^3} - \frac{6\sqrt{1 + \xi^2}\sigma}{(-1 + \xi\sigma)^2} - \frac{6\sqrt{1 + \xi^2}\sigma}{-1 + \xi\sigma} \right. \\ & + \frac{\sigma(6 + 11\sigma^2 + 2\sigma^4)}{(1 + \sigma^2)^2} \\ & + \frac{\left(\sqrt{1 + \xi^2}\sigma(6 + 11\sigma^2 + 2\sigma^4 - 3\xi\sigma(5 + 9\sigma^2 + 2\sigma^4) + \xi^2\sigma^2(11 + 20\sigma^2 + 6\sigma^4))\right)}{\left((-1 + \xi\sigma)^3(1 + \sigma^2)^2\right)} \\ & - 6\sinh^{-1}[\xi] - \frac{3(2 + 5\sigma^2 + 4\sigma^4)\ln[1 - \xi\sigma]}{(1 + \sigma^2)^{\frac{5}{2}}} - \frac{3(2 + 5\sigma^2 + 4\sigma^4)\ln[\sigma + \sqrt{1 + \sigma^2}]}{(1 + \sigma^2)^{\frac{5}{2}}2} \\ & \left. + \frac{3(2 + 5\sigma^2 + 4\sigma^4)\ln\left[\xi + \sigma + \sqrt{1 + \xi^2}\sqrt{1 + \sigma^2}\right]}{(1 + \sigma^2)^{\frac{5}{2}}} \right\}.\end{aligned}\tag{16}$$

The total energy density ϵ is then obtained from the equation:

$$\epsilon = \rho c^2 + \epsilon_e\tag{17}$$

6 *Bernaldez, Abac, Otadoy*

where the mass density ρ is equal to:

$$\rho(\xi) = m_u \mu_e n = \frac{K}{qc^2} \tilde{N}(\xi) \quad (18)$$

The variable q here is equal to $\frac{m_e}{(\mu_e m_u)}$, where $m_u = 1.6605 \times 10^{-24}$ g, which is the atomic mass, and $\mu_e = \frac{A}{Z} = 2$, where A is the mass number and Z is the atomic number. The total energy density is:

$$\epsilon = \frac{K}{q} \tilde{N}(\xi) + K \tilde{\epsilon}_e = \frac{K}{q} \tilde{\epsilon}, \quad (19)$$

where $\tilde{\epsilon}$ is the dimensionless total energy density and is given by:

$$\tilde{\epsilon} = \tilde{N}(\xi) + q \tilde{\epsilon}_e \quad (20)$$

It should be noted that the LGUP-modified equations (12), (13), and (14) are

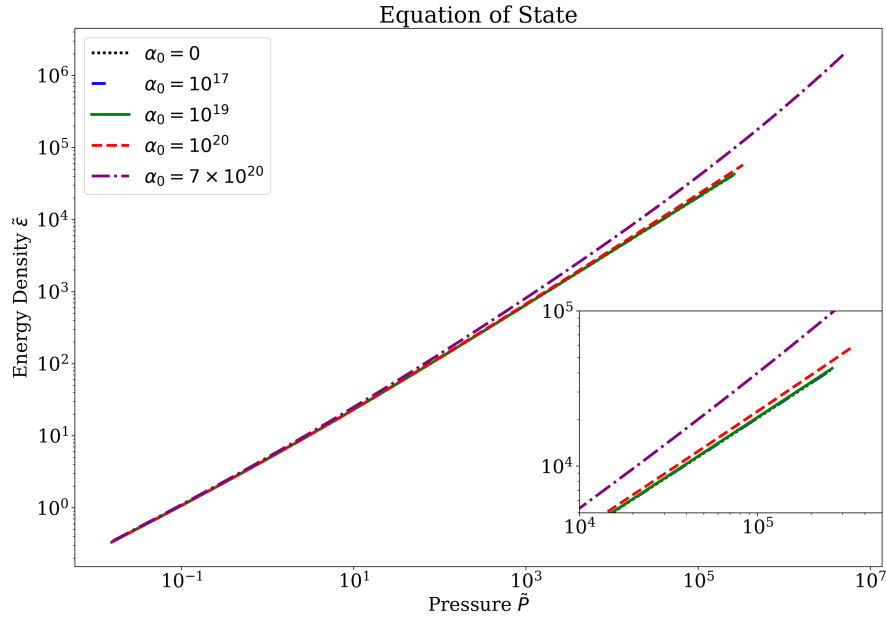


Fig. 1. Equation of State of Linear GUP-modified White Dwarfs

singular at $\tilde{p} = \frac{1}{\sigma}$. This implies that there is a constraint with regards the momentum values such that $0 < \tilde{p} < \frac{1}{\sigma}$. This maximum \tilde{p} is of the same order of magnitude as ξ as shown in Ref. 1,34. Since ξ is the Fermi momentum for a white dwarf, the linear-GUP structure equation for the white dwarf can be safely calculated in the range said range, which is sufficient in obtaining the mass-radius relation of white dwarfs. Equations (16) and (20) will be used to generate the plot for the equation

of state for the linear-GUP-modified white dwarfs. The equation of state for the zero-temperature ideal electron gases for various values of the GUP parameter α_0 is shown in Figure 1. From the plots of the equations of states, it can be seen that the plot for $\alpha_0 = 10^{17}$ and $\alpha_0 = 0$ are practically the same, which means that the effect of linear GUP for a GUP parameter of 10^{17} is negligible. It can also be seen from the plot that there is a slight increase in the slope for $\alpha_0 = 10^{19}$, which can be seen clearly for larger values of the pressure \tilde{P} . A more notable increase of the slope is visible for both $\alpha_0 = 10^{20}$ and $\alpha_0 = 7 \times 10^{20}$ for large values of \tilde{P} , which means that the effect of linear GUP is significant for $\alpha_0 = 10^{19}$ and $\alpha_0 = 10^{20}$, and is much greater for $\alpha_0 = 7 \times 10^{20}$. From the plots, we can say that the EOS softens with the presence of LGUP.

3. White Dwarf Structure

In this section, we use the results from Chapter 2 to modify the TOV equations and obtain the mass-radius relations of white dwarfs with LGUP.

3.1. Tolman-Oppenheimer-Volkoff (TOV) Equations

The structure of white dwarfs can be approximated by the Newtonian equations of stellar structure. However, for the most massive white dwarfs, which are affected by GUP, general relativity (GR) has to be taken into account. From the Einstein field equations, and using the metric $ds^2 = e^\nu c^2 dt^2 - e^\mu dr^2 - r^2(d\theta^2 + \sin^2\theta d\phi^2)$, one can obtain the structure of GR known as the TOV given by:^{1,13,27,28}

$$\frac{dP}{dr} = -\frac{G}{c^2 r}(\epsilon + P)\frac{m + \frac{4\pi r^3}{c^2}}{r - \frac{2GM}{c^2}}, \quad P(r=0) = P_c, \quad P(r=R_\star) = 0, \quad (21)$$

$$\frac{dm}{dr} = \frac{4\pi}{c^2}\epsilon r^2, \quad m(r=0) = 0, \quad m(r=R_\star) = M_\star, \quad (22)$$

where (21) is the statement of hydrostatic equilibrium, while (22) is the mass continuity equation together with their boundary conditions. R_\star and the M_\star are the star radius and star mass, respectively. From the boundary conditions, we can see that the pressure is greatest P_c at the center of the star and gradually decreases to zero at $r = R_\star$. On the other hand, the mass at the center of the star is zero, and as we move away from the center of the star, the star accumulates mass until it reaches a mass equal to M_\star at $r = R_\star$.

We can then re-express the TOV equations (21) and (22) in terms of dimensionless quantities ξ, η , and v modified with LGUP. With this, we start with:

$$\frac{d\tilde{P}}{d\eta} = \frac{d\tilde{P}}{d\xi} \frac{d\xi}{d\eta} \rightarrow \frac{d\xi}{d\eta} = \frac{1}{\frac{d\tilde{P}}{d\xi}} \frac{d\tilde{P}}{d\eta}, \quad (23)$$

8 *Bernaldez, Abac, Otadoy*

where $\frac{d\tilde{P}}{d\xi}$ and $\frac{d\tilde{P}}{d\eta}$ are:

$$\frac{d\tilde{P}}{d\xi} = \frac{\xi}{\sqrt{1+\xi^2}} \tilde{N}(\xi) \quad (24)$$

and

$$\frac{d\tilde{P}}{d\eta} = \frac{-(\tilde{\varepsilon} + q\tilde{P})}{\eta} \frac{v + q\tilde{P}\eta^3}{\eta - 2qv} \quad (25)$$

respectively. We can then obtain the dimensionless equation for $\frac{d\xi}{d\eta}$

$$\frac{d\xi}{d\eta} = -\frac{\sqrt{1+\xi^2}}{\xi} \frac{1 + q\sqrt{1+\xi^2}}{\eta} \frac{v + q\tilde{P}\eta^3}{\eta - 2qv}, \quad \xi(\eta = 0) = \xi_c, \quad \xi(\eta = \eta_R) = 0. \quad (26)$$

Equation (22) can then be rewritten in terms of dimensionless quantities and is given by:

$$\frac{m_0 dv}{r_0 d\eta} = \frac{4\pi}{c^2} \frac{K}{q} \tilde{\varepsilon} (\eta r_0)^2, \quad (27)$$

which can be simplified into:

$$\frac{dv}{d\eta} = \frac{4\pi}{c^2} \frac{K}{q} \frac{1}{m_0} \tilde{\varepsilon} r_0^3 \eta^2 = \frac{4\pi}{c^2} \frac{K}{q} \frac{1}{m_0} \tilde{\varepsilon} \eta^2 \frac{\left(\frac{qc^2}{\sqrt{4\pi G K}}\right)^3}{\frac{q^2 c^4}{G \sqrt{4\pi G K}}}, \quad (28)$$

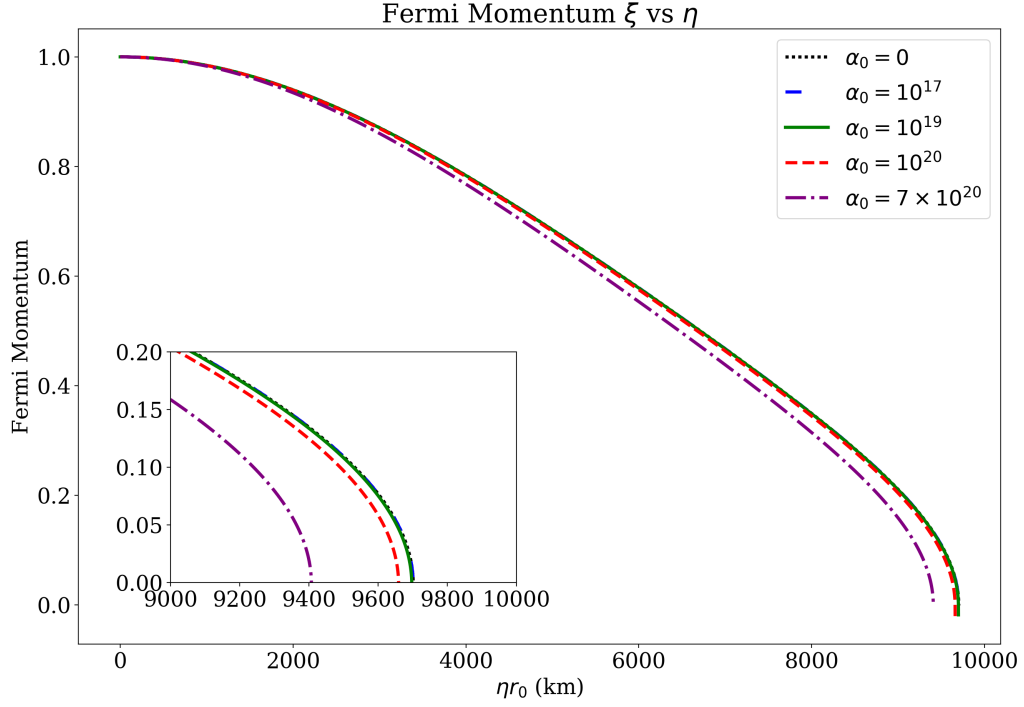
and we finally obtain:

$$\frac{dv}{d\eta} = \tilde{\varepsilon} \eta^2, \quad v(\eta = 0) = 0, \quad v(\eta = \eta_R) = v_R \quad (29)$$

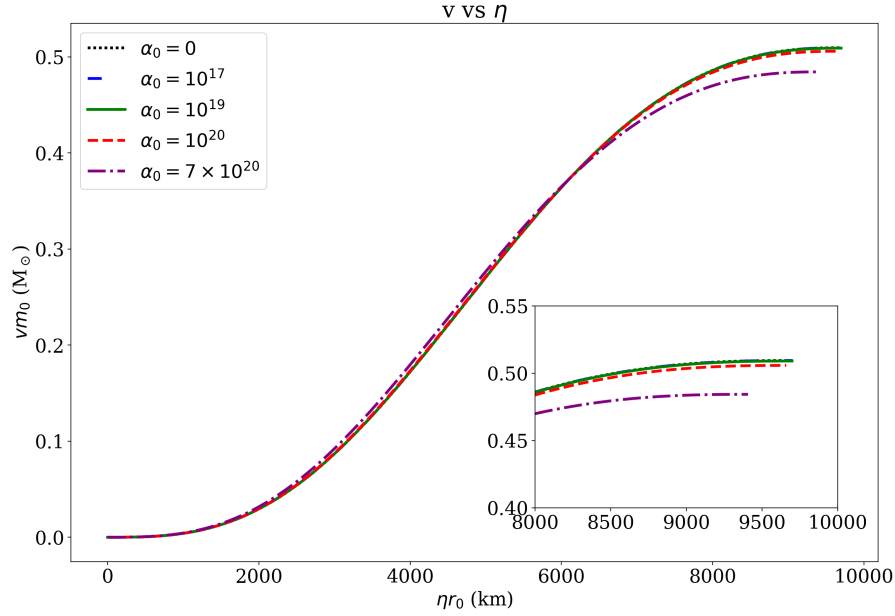
where ξ is the dimensionless Fermi momentum (or momentum density) defined in (11), $v = \frac{m}{m_0}$, $\eta = \frac{r}{r_0}$, $m_0 = \frac{q^2 c^4}{G \sqrt{4\pi G K}}$, $r_0 = \frac{qc^2}{\sqrt{4\pi G K}}$, and v_R and η_R are the dimensionless star mass and star radius, respectively. Notice that in this case, we have redefined our TOV equations in terms of the Fermi momentum ξ instead of the usual pressure p , for convenience in dealing with the dynamical instability analysis later on. This is different from approach of Ref. 1, but should nevertheless yield the same results.

3.2. Mass-Radius Relations

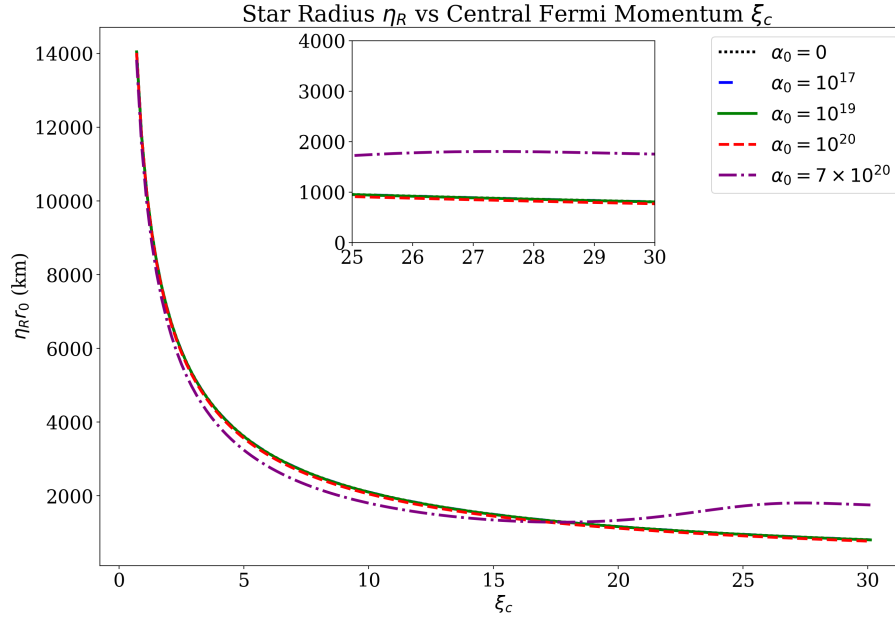
Figure 2 shows the Fermi momentum versus η plot for both the LGUP-modified white dwarfs and the white dwarf with no linear GUP corrections. The figure shows that the Fermi momentum of the star decreases from the center of the white dwarf and vanishes at the radius of the white dwarf. We also see that the GUP parameter of 10^{17} appears to have a negligible effect on the white dwarf. On the other hand, the white dwarfs with $\alpha_0 = 10^{19}$, 10^{20} , and 7×10^{20} have variations to their plots with respect to the ideal case, where they have smaller final star radius than the white dwarfs with no linear GUP effects. This trend is more evident when looking

Fig. 2. ξ vs η Plot

at the GUP parameter of 7×10^{20} , where the plot is shown to have a value of η_R . Figure 3 shows the v versus η plot for varying values of the GUP parameter α_0 . The plot shows similar results as the previous figure in the sense that the plot with $\alpha_0 = 10^{17}$ shows negligible effects as it shows a similar trend to the plot for $\alpha_0 = 0$. On the other hand, $\alpha_0 = 10^{19}$, and $\alpha_0 = 10^{20}$ show significant linear GUP effects on the white dwarfs, where linear GUP appears to decrease the final mass of the white dwarf, which is notable at larger values of η . The plot also shows that for $\alpha_0 = 7 \times 10^{20}$, v_R is much smaller compared to those with smaller α_0 . The star radius η_R versus central Fermi momentum plot ξ_c (shown in Figure 4) indicates that various values of ξ_c correspond to different star radius values. Larger values of ξ_c corresponds to a smaller star radius, while smaller values of ξ_c corresponds to a more prominent star radius. This checks out with the fact that a larger ξ_c indicates a more compact object, thus, a smaller radius. It should be noted that for a GUP parameter of 7×10^{20} , η_R decreases faster at low values of ξ_c compared with smaller α_0 . However, η_R reaches a minimum at some ξ_c before increasing for larger values of ξ_c , while for the other α_0 , η_R just decreases in value in this range of central fermi momentum $\xi_c \in [0, 25]$. Note that the range of the central Fermi momenta that

Fig. 3. v vs η Plot

we used is well within the constraints we placed for the Fermi momentum. This is sufficient to describe the trend of the mass radius relation, as well as the dynamical instability analysis for LGUP-modified white dwarfs. Figure 5 corresponds to the star mass versus the central Fermi momentum plot, which shows the noticeable effects of GUP on the star mass. The plot shows that the effect of GUP is to decrease the maximum star mass, that is the Chandrasekhar limit. The GUP parameter $\alpha_0 = 10^{17}$ exhibits negligible effects to the maximum star mass, while $\alpha_0 = 10^{19}$ shows a noticeable decrease and a drastic decrease of the maximum star mass for $\alpha_0 = 10^{20}$. For $\alpha_0 = 7 \times 10^{20}$, v_R drastically decreases smaller values of ξ_c , however, for larger values of Fermi momentum ξ_c , v_R is shown to increase. The mass-radius relations can be seen in Figure 6, together with observational data taken from Ref. 34 which contains the parametric plots between star radius and star mass. The plots show that as the star radius decreases, the star mass increases, which means that the white dwarf is heavier when it's dimensionally smaller, demonstrating its compact nature. Examining the plot from the largest star radius decreasing towards zero (right to left), we see that the star mass eventually reaches a maximum value, before decreasing towards zero radius. The plots also show that for larger values of the GUP parameter α_0 , the maximum mass is smaller, while $\alpha_0 = 10^{17}$ shows that the effects of the GUP parameter are negligible. There is also a larger limiting radius, which is the radius by which the star reaches its maximum mass, for the larger GUP

Fig. 4. η_R vs ξ

parameters. In addition, for a GUP parameter of 7×10^{20} , as the final radius of the white dwarf becomes smaller, the mass increases but eventually decreases after reaching the maximum mass of the white dwarf. However, at the lower values of the final radius, the plot starts to spiral, where both the final mass and final radius increases. The table shows the value of maximum mass and minimum radius of

α_0	$v_R (M_\odot)$	$\eta_R(\text{km})$
0	1.411	1077.129
10^{17}	1.411	1077.129
10^{19}	1.393	1269.338
10^{20}	1.289	2033.731
7×10^{20}	0.984	3409.005

the white dwarf for every α_0 . We see that for $\alpha_0 = 10^{17}$ are similar with $\alpha_0 = 0$, which means that the effect of LGUP is negligible. In addition, we can see that the maximum value of v_R decreases with increasing value of the GUP parameter. On the other hand, the corresponding η_R increases when α_0 is larger. This means that for larger values of the GUP parameter α_0 , LGUP-modified white dwarfs have a lower mass limit. The behaviours observed in the structure equations and mass

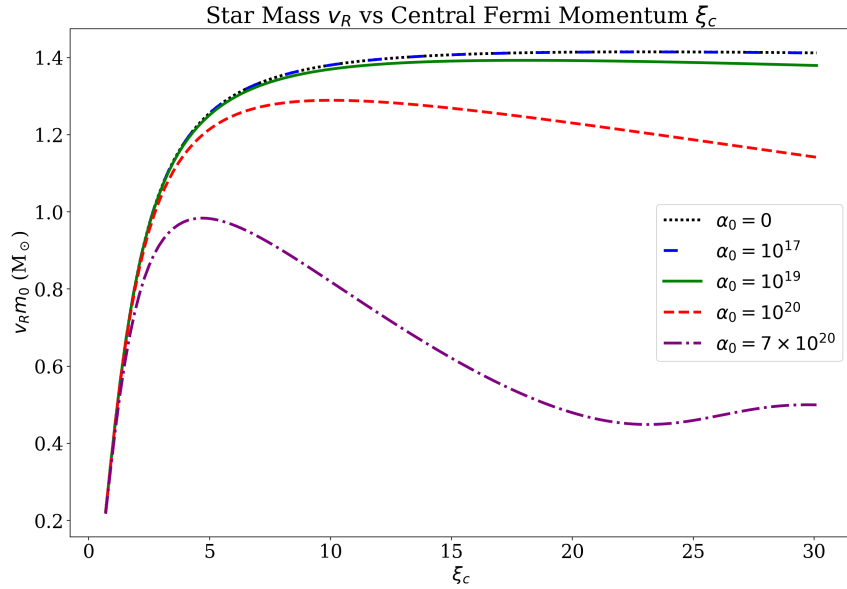


Fig. 5. ν_R vs ξ

radius relations are similar to those obtained from Ref. 1, albeit using a different approach. We will see in the next section that white dwarfs beyond the maximum mass limit are unstable configurations.

4. Dynamical Instability Analysis

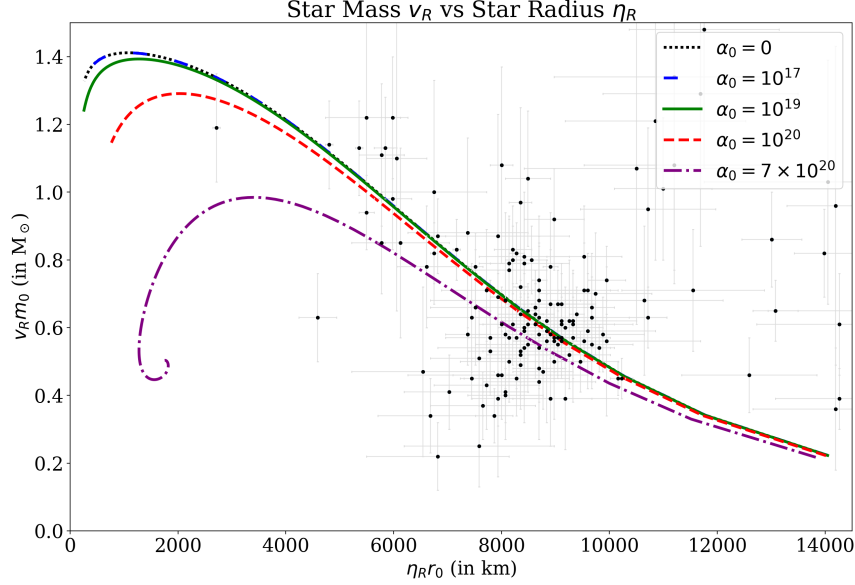
In Subsection 4.1, we review some general results in analyzing the dynamical instability of white dwarfs, following the procedures laid out by Ref. 11–15, 29–32. In Subsection 4.2, we present our own derived expressions for the dynamical instability analysis containing LGUP modifications.

4.1. Radial Oscillations and Dynamical Instability of White Dwarfs

For the dynamical stability analysis, we start with the metric interior of the star, which can be expressed as:^{13, 29–31}

$$ds^2 = e^{\nu+\delta\nu} c^2 dt^2 - e^{\mu+\delta\mu} dr^2 - r^2(d\theta^2 + \sin^2\theta d\phi^2). \quad (30)$$

From the equation, $\nu(r)$ and $\mu(r)$ here refers to the equilibrium metric potentials, while $\delta\nu(r, t)$ and $\delta\mu(r, t)$ refers to the perturbations due to small radial Lagrangian displacements $\zeta(r, t)$ given by $\zeta(r, t) = r^{-2} e^{\frac{\nu}{2}\psi(r)} e^{i\omega t}$ which induces perturbations


 Fig. 6. η_R vs v_R

$\delta P(r, t)$ and $\delta \epsilon(r, t)$. The radial oscillation equation can then be obtained in the Sturm-Liouville form and is given by:^{13, 32}

$$\frac{d}{dr} \left(U \frac{d\psi}{dr} \right) + \left(V + \frac{\omega^2}{c^2} W \right) \psi = 0, \quad (31)$$

With the boundary conditions $\psi = 0$ at $r = 0$, and $\delta P = -e^{\frac{\nu}{2}} \left(\frac{\gamma P}{r^2} \right) \frac{d\psi}{dr} = 0$ at $r = R$, the terms in equation (3.2) are:

$$U(r) = e^{\frac{(\mu+3\nu)}{2}} \frac{\gamma P}{r^2}, \quad (32)$$

$$V(r) = -4 \frac{e^{\frac{\mu+3\nu}{2}}}{r^3} \frac{dP}{dr} - \frac{8\pi G}{c^4} \frac{e^{\frac{3\mu+\nu}{2}}}{r^2} P(P + \epsilon) + \frac{e^{\frac{\mu+3\nu}{2}}}{r^2} \frac{1}{P + \epsilon} \left(\frac{dP}{dr} \right)^2, \quad (33)$$

$$W(r) = \frac{e^{\frac{3\mu+\nu}{2}}}{r^2} (P + \epsilon), \quad (34)$$

where γ is the adiabatic index equal to:

$$\gamma = \frac{\epsilon + P}{P} \left(\frac{dP}{d\epsilon} \right). \quad (35)$$

Distributing ψ to equation (31) and then integrating, where we let $\psi' = \frac{d\psi}{dr}$, we obtain:

$$J[\psi] = \int_0^R U\psi'^2 - V\psi^2 - \frac{\omega^2}{c^2} W\psi^2 dr. \quad (36)$$

Minimizing equation (40) with respect to ψ , we can then obtain the Sturm-Liouville equation in equation (31), which means we have a variational basis for determining the lowest characteristic eigenfrequency and is expressed as:

$$\frac{\omega_0^2}{c^2} = \min_{\psi(r)} \frac{\int_0^R (U\psi'^2 - V\psi^2) dr}{\int_0^R W\psi^2 dr} \quad (37)$$

From equation (43), we will then obtain a set of ω_0^2 values corresponding to a range of central Fermi momentum ξ . A star with an ω_0^2 that is greater than zero means that the star is stable, while a star that has a negative ω_0^2 value means that dynamical instability is present for that certain central Fermi momentum value. The trial function ψ of the fundamental mode can be approximated in the form $\psi(r) = c_0 r^{313, 29, 30, 33}$. The equation for the central mass density can be found in equation (18). With this, the mass density at which the white dwarf shows gravitational collapse will be the critical density ρ_c^* and can be identified with the zero eigenfrequency solution of the equation.

The interior Schwarzschild metric potentials, which satisfy Einstein's field equations, are given by^{13, 27, 28}

$$e^{-\mu(r)} = 1 - \frac{2GM}{c^2 r}, \quad (38)$$

and

$$e^\nu = \left(1 - \frac{2GM}{c^2 R}\right) \left(\exp \left[-2 \int_0^{P(r)} \frac{dP}{\varepsilon + P}\right]\right). \quad (39)$$

4.2. *Dynamical Instability Analysis for LGUP-modified White Dwarfs*

We then rewrite the expressions in Section 4.1, this time taking into account the dimensionless quantities we defined in Chapter 2 together with LGUP modification. The dimensionless adiabatic index $\tilde{\gamma}$ can be obtained using the definition of $\frac{dP}{d\varepsilon}$ given by:

$$\frac{dP}{d\varepsilon} = \left[\frac{\xi^2 (1 - \xi\sigma)}{3\sqrt{1 - \xi^2} (1 + q\sqrt{1 + \xi^2})} \right], \quad (40)$$

where $\tilde{\gamma}$ will be:

$$\tilde{\gamma} = \frac{\frac{K}{q}\tilde{\varepsilon} + K\tilde{P}}{K\tilde{P}} \left(\frac{d\tilde{P}}{d\tilde{\varepsilon}} \right) = \frac{\tilde{\varepsilon} + q\tilde{P}}{\tilde{P}} \left[\frac{\xi^2 (1 - \xi\sigma)}{3\sqrt{1 - \xi^2} (1 + q\sqrt{1 + \xi^2})} \right], \quad (41)$$

and can be simplified to:

$$\tilde{\gamma} = N\xi^2 \frac{(1 - \sigma \xi)}{3\tilde{P}\sqrt{1 + \xi^2}} \quad (42)$$

Equation (37) can then be rewritten in terms of dimensionless quantities given by:¹³

$$\omega_0^2 = \left(\frac{qc^2}{r_0^2} \right) \frac{I + J}{K}, \quad (43)$$

where the equations for I , J , and K , are given by:

$$I = \int_0^{\eta_R} e^{(\mu+3\nu)/2} \frac{\gamma \tilde{P}}{\eta^2} \psi'^2 d\eta, \quad (44)$$

$$J = \int_0^{\eta_R} \frac{e^{(\mu+3\nu)/2}}{\eta^2} \left[\frac{4}{\eta} \frac{d\tilde{P}}{d\eta} + 2qe^\mu \tilde{P} (\tilde{\varepsilon} + q\tilde{P}) - \frac{q}{\tilde{\varepsilon} + q\tilde{P}} \left(\frac{d\tilde{P}}{d\eta} \right)^2 \right] \psi^2 d\eta, \quad (45)$$

$$K = \int_0^{\eta_R} e^{(3\mu+\nu)/2} \frac{\tilde{\varepsilon} + q\tilde{P}}{\eta^2} \psi^2 d\eta, \quad (46)$$

respectively. The interior Schwarzschild metric potential from Equations (38) and (39) can also be re-expressed in terms of dimensional quantities given by:

$$e^{-\mu} = 1 - \frac{2Gvm_0}{c^2\eta r_0} = 1 - \frac{2Gv \frac{(qc^2)^2}{(G^{3/2}\sqrt{4\pi K})}}{c^2\eta \frac{qc^2}{\sqrt{4\pi G K}}} = 1 - 2q \frac{v}{\eta} \quad (47)$$

and

$$e^\nu = \left(1 - 2q \frac{v_R}{\eta_R} \right) \left(\exp \left[-2 \int_0^{P(r)} \frac{qK d\tilde{P}}{K(\tilde{\varepsilon} + q\tilde{P})} \right] \right), \quad (48)$$

which can be simplified into

$$e^{\nu(\eta)} = \left(1 - 2q \frac{v_R}{\eta_R} \right) \left[\frac{(1 + q)^2}{(1 + q\sqrt{1 + \xi^2})^2} \right]. \quad (49)$$

Plotting the numerical integrations from the equations above gives us the eigenfrequency ω_0^2 versus central density ρ_c plot for varying values of the GUP parameter α_0 shown in Figure 7. From the plot, we can see that white dwarfs with central densities $\rho_c \lesssim 10^7 \text{ g cm}^{-3}$ have overlapping plots, which means that the effect of the GUP parameter does not have a notable impact on the white dwarfs in the indicated range of central densities. This also means that all the values of the GUP parameter in the range of $0 \leq \alpha_0 \leq 10^{17}$ will yield similar results, which are overlapping plots with the ideal case ($\alpha_0 = 0$) and have approximately the same value

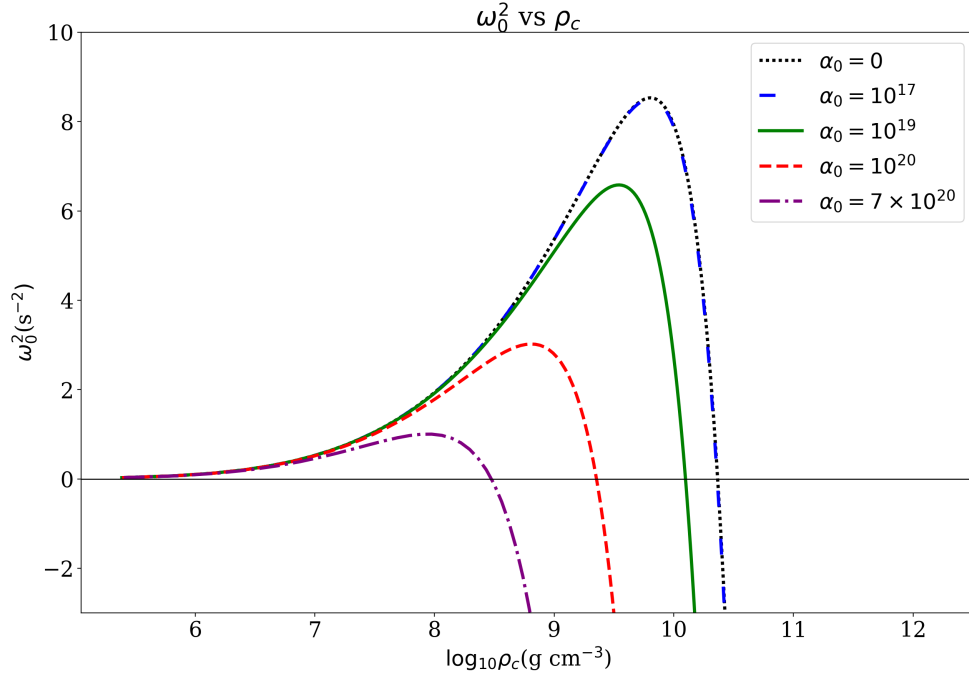


Fig. 7. Eigenfrequency of the fundamental mode ω_0^2 versus central mass density ρ_c for different values of α_0

of the central density by which gravitational collapse begins. This is also apparent in the mass radius relation where low mass white dwarfs are not significantly affected by GUP. The plots of the different GUP parameters start to deviate in the higher density regime, where a larger GUP parameter such as for $\alpha_0 = 10^{20}$, $\alpha_0 = 10^{19}$, and $\alpha_0 = 7 \times 10^{20}$ deviates at a lower ρ_c than the other values of α_0 . The GUP parameter 7×10^{20} also shows that the maximum value of $\omega_0^2 \approx 1$ and is shown to decrease immediately from there at smaller values of the central density. On the other hand, a GUP parameter equal to 10^{17} has negligible effects on the white dwarfs. A larger GUP parameter shows that the white dwarf has a smaller central density by which its eigenfrequency reaches a maximum value. This is true for GUP parameters 10^{19} , 10^{20} , and 7×10^{20} , while the plot of $\alpha_0 = 10^{17}$ has a large ω_0^2 value, and corresponding ρ_c^* value. However, it should be noted that all values of the GUP parameter yield similar behaviors, which show a descending value for eigenfrequency in higher central densities. This means that there exists a zero eigenfrequency solution at critical central densities ρ_c^* for different values of the GUP parameter, beyond which, at $\omega_0^2 \leq 0$ the white dwarfs will undergo gravitational collapse. Table 2 shows the values of the critical mass density ρ_c^* , star mass,

α_0	ρ_c^*	$v_R (M_\odot)$	$\eta_R(\text{km})$
0	1.036×10^{11}	1.415	1025.493
10^{17}	1.036×10^{11}	1.415	1033.486
10^{19}	1.009×10^{11}	1.396	1243.393
10^{20}	9.332×10^{10}	1.291	2031.892
7×10^{20}	8.433×10^{10}	0.985	3407.039

star radius for various values of α_0 . The table shows that the critical mass density values, star radius, and star mass are similar for $\alpha_0 = 0$ and $\alpha_0 = 10^{17}$. However, for GUP parameter $\alpha_0 = 10^{19}$, $\alpha_0 = 10^{20}$, and $\alpha_0 = 7 \times 10^{20}$, the critical mass density and final mass are shown to decrease with increasing values of the GUP parameter. This means that larger values of the GUP parameter reduces the final mass before it undergoes gravitational collapses. On the other hand, the larger the GUP parameter, the larger the final radius of the white dwarf before it collapses. Since the final mass of the white dwarf decreases with increasing values of the GUP parameter, the Chandrasekhar mass limit of $1.42M_\odot$ remains unaltered. In addition, the maximum value of the critical central density from the table is much smaller than the nuclear matter density of around $10^{14} \text{ g cm}^{-3}$, thus the assumption of a free fermionic equation of state holds true to the stable regime of the white dwarfs. Comparing the table above to Table 1, we can see that the corresponding v_R and η_R values of the peaks from the mass-radius relation plot in Figure 6 are practically similar to Table 2 for the same values of α_0 . This means that from the mass-radius relation plots, we can identify that instability occurs for larger α_0 values at larger star radius and smaller star mass. With this, we know that dynamical instability happens after reaching the maximum mass of the star, when examining the plots from the largest star radius decreasing towards zero. When the radius of the star is smaller than the corresponding radius of the star after reaching its maximum mass, dynamical instability occurs. Figure 8 shows the complete plot of ω_0^2 versus central mass density ρ_c for $\alpha_0 = 7 \times 10^{20}$, which shows all the values of ω_0^2 below zero. From this plot, we can see that ω_0^2 decreases from zero, until it reaches the minimum value of ω_0^2 , where it increases again from there. This behavior confirms the spiraling that occurs in the mass-radius plot.

5. Conclusions and Recommendations

The mass-radius relations plots from Ref. 1 are successfully replicated in this study. The results of the mass-radius relations and dynamical instability analysis show that dynamical instability sets in at different values of η_R and v_R for various values of the GUP parameter α_0 . The mass-radius relations plot shows us that after reaching a certain maximum mass, the white dwarfs will become unstable and will continuously decrease its mass and radius due to instability. On the other hand, based on the results from dynamical instability analysis, we find that the dynamical instability sets in for all values of the GUP parameters α_0 , albeit at different mass limits.

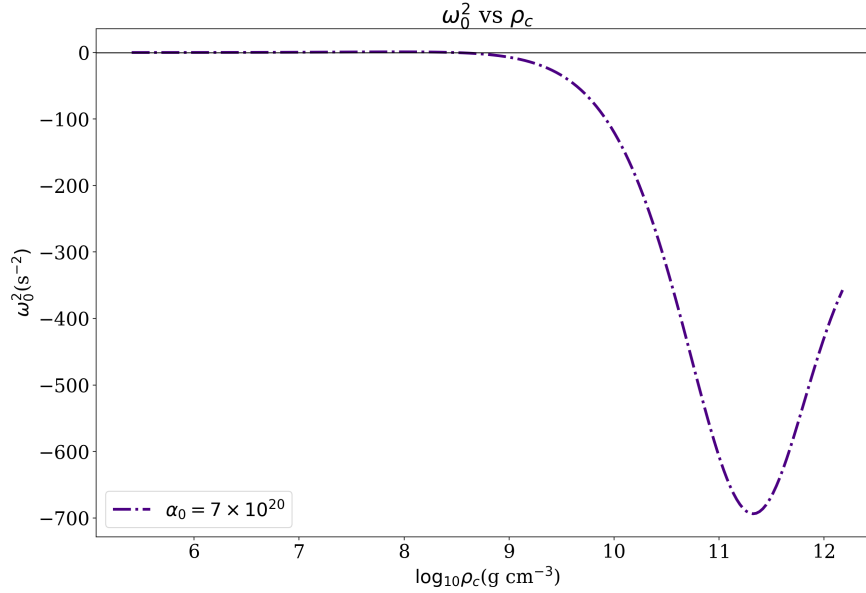


Fig. 8. Eigenfrequency of the fundamental mode ω_0^2 versus central mass density ρ_c for different values of α_0

This verifies the results obtained from the mass-radius relations plots. In addition, we find that the Chandrasekhar mass limit is preserved for LGUP-modified white dwarfs as seen from the onset of gravitational collapse, where as we increase the value of α_0 , the mass limit will tend to decrease. The results show that when the eigenfrequency of the fundamental mode ω_0^2 is plotted against the central density ρ_c for various values of the GUP parameter α_0 , the eigenfrequencies ω_0^2 continuously decrease up to the critical central density ρ_c^* indicating gravitational collapse.

It can be observed that the eigenfrequency for a GUP parameter $\alpha_0 = 10^{17}$ coincides with the plot for the ideal case, which has no GUP correction. With this, for GUP parameters within the range of $\alpha_0 = 0$ and $\alpha_0 = 10^{17}$, the critical central density ρ_c^* for the onset of gravitational collapse will be approximately the same. For values of the GUP parameter in the range $0 \leq \alpha_0 \leq 10^{17}$, their corresponding mass-radius relation plot shows maximal points corresponding to the Chandrasekhar mass limit at around $1.42M_\odot$. This accurate for numerous astronomical observations in the case of white dwarfs and other compact objects. On the other hand, larger values of α_0 is shown to have a lower maximum value when compared to α_0 values less than 10^{17} , which implies that the mass limit by which instability sets in is lower. It is given that upon reaching a mass beyond the Chandrasekhar mass limit, the star would collapse and will form a more compact object.

With this, the LGUP-modification supports gravitational collapse by decreasing the Chandrasekhar mass limit of the white dwarf. This is opposite to the results obtained when using QGUP, where at some values of the GUP parameter β_0 , the white dwarf will remain stable at masses beyond the Chandrasekhar mass limit.

The works of Ref. 13 suggested that the GUP parameter β can be negative. This means that future studies can explore the effects of a negative LGUP parameter α_0 . In addition, dynamical instability analysis can be used for other astronomical systems such as neutron stars. Dynamical instability analysis can be used to analyze the radial oscillations of neutron stars and compare its behavior to other compact objects when modified by LGUP. Lastly, future studies can explore using other numerical methods for solving the equations above to improve the accuracy and efficiency of the calculations. With this, using larger values of α_0 would be possible, which will be helpful in identifying the upper bound of the LGUP parameter to be used for white dwarfs.

Acknowledgments

The authors thank the Department of Science and Technology for providing financial support for this project.

References

1. Abac, A. & Esguerra, J.P., & Otadoy, R.E., (2020). Modified structure equations and mass–radius relations of white dwarfs arising from the linear generalized uncertainty principle. *International Journal of Modern Physics D*, 30(01), 2150005.
2. Abac, A. G., & Esguerra, J. P. H. (2021). Implications of the generalized uncertainty principle on the Walecka model equation of state and neutron star structure. *International Journal of Modern Physics D*, 30(08), 2150055.
3. Blau, M. (2009). String theory as a theory of quantum gravity: a status report, *Gen. Relativ. Gravit.* 41, 743-755
4. Gross, D., Mende, P. (1988). String theory beyond the Planck scale, *Nucl. Phys. B* 30, 407-454
5. Konishi, K., Paffuti, G., Provero, P. (1990). Minimum physical length and the generalized uncertainty principle in string theory, *Phys. Lett. B* 234 276-284
6. Maggiore, M. (1993). A generalized uncertainty principle in quantum gravity, *Phys. Lett. B* 304 65-69
7. Scardigli, F. (1999). Generalized Uncertainty Principle in Quantum Gravity from Micro-Black Hole Gedanken Experiment, *Phys. Lett. B* 452, arxiv: 9904025 [hep-th]
8. Cortes, J., Gamboa, J. (2005). Quantum Uncertainty in Doubly Special Relativity. *Phys. Rev. D* 71 (065015)
9. Ali, A. F. (2011). *Minimal length in quantum gravity, equivalence principle and holographic entropy bound*. <https://arxiv.org/abs/1101.4181>
10. Ali, A., Das, S., Vagenas, E. (2012). The generalized uncertainty principle and quantum gravity phenomenology. *The Twelfth Marcel Grossmann Meeting: On Recent Developments in Theoretical and Experimental General Relativity, Astrophysics and Relativistic Field Theories* 2407-2409

11. Mathew, A., & Nandy, M. K. (2020). Prospect of Chandrasekhar's limit against modified dispersion relation. *General Relativity and Gravitation*, 52(4).
12. Mathew, A. & Nandy, M. K. (2018). *Ann. Phys.* 393 184.
13. Mathew, A., & Nandy, M. K. (2021). Existence of Chandrasekhar's limit in generalized uncertainty white dwarfs. *Royal Society Open Science*, 8(6), 210301.
14. Chandrasekhar, S. (1967) *An Introduction to the Study of Stellar Structure*. New York: Dover, pp. 84-182.
15. Chandrasekhar, S. (1931) The Maximum Mass of Ideal White Dwarfs, *Astrophys. J.* 74 81-82.
16. Tawfik, A. (2014) Diab. Generalized uncertainty principle: Approaches and applications, *Int. J. Mod. Phys. D* 23.
17. Tawfik, A. Diab. (2015) A review of the generalized uncertainty principle, *Rep. Prog. Phys.* 78.
18. Kempf, A., Mangano, R. (1995). Mann. Hilbert space representation of the minimal length uncertainty relation, *Phys. Rev. D* 52 1108-1118
19. Silbar, R., Reddy, S. (2004) Neutron stars for undergraduates, *Am. J. Phys.* 72 892-905
20. Kilic, M., et. al. (2007). The Lowest Mass White Dwarf, *Astrophys. J.* 660 1451-1461
21. Kepler, S., et. al. (2007). White dwarf mass distribution in the SDSS, *Mon. Not. R. Astron. Soc.* 375 1315-1324
22. Schutz, B. (2003). Gravity from Ground Up, *Cambridge: Cambridge University Press*, ISBN 0-521-45506-5
23. Moussa, M. (2015). Effect of Generalized Uncertainty Principle on Main-Sequence Stars and White Dwarfs, *Adv. High Energy Phys.*
24. Moussa, M. (2017). Quantum Gravity Corrections in Chandrasekhar Limits, *Physica A* 465, arXiv: 1511.06183v2 [physics.gen-ph]
25. Bertolami, O., Zarro, C. (2010). Towards a noncommutative astrophysics, *Phys. Rev. D* 81, (025005)
26. Nozari, K., Etemadi, A. (2012). Minimal length, maximal momentum, and Hilbert space representation of quantum mechanics, *Phys. Rev. D* 85, 10
27. Tolman, R.C. (1939). Static solutions of Einstein's field equations for spheres of fluid. *Phys. Rev.* 55, 364-373. (doi:10.1103/PhysRev.55.364)
28. Oppenheimer, J.R., Volkoff, G.M. (1939). On massive neutron cores. *Phys. Rev.*
29. Chandrasekhar, S. (1964). The dynamical instability of gaseous masses approaching the Schwarzschild limit in general relativity. *Astrophys. J.* 140, 417. (doi:10.1086/147938)
30. Chandrasekhar, S., Tooper, R.F. (1964). The dynamical instability of white-dwarf configurations approaching the limiting mass. *Astrophys. J.* 139, 1396. (doi:10.1086/147883)
31. Mathew, A., Nandy, M.K. (2020). Prospect of Chandrasekhar's limit against modified dispersion relation. *Gen. Relativ. Grav*
32. Bardeen, J.M., Thorne, K.S., Meltzer, D.W. (1966). A catalogue of methods for studying the normal modes of radial pulsation of general-relativistic stellar models. *Astrophys. J.* 145, 505. (doi:10.1086/148791)
33. Wheeler, J.C., Hansen, C.J., Cox, J.P. (1968). General relativistic instability in white dwarfs. *Astrophys. J. Lett.* 2, 253
34. Bedard, A., Bergeron, P., and Fontaine, G. (2017). Measurements of physical parameters of white dwarfs: A test of the mass-radius relation. *Astrophys. J.* 848